

Regional Climate Modeling over the Maritime Continent. Part II: New Parameterization for Autoconversion of Convective Rainfall

REBECCA L. GIANOTTI AND ELFATIH A. B. ELTAHIR

Ralph M. Parsons Laboratory, Massachusetts Institute of Technology, Cambridge, Massachusetts

(Manuscript received 19 March 2013, in final form 9 August 2013)

ABSTRACT

This paper describes a new method for parameterizing the conversion of convective cloud liquid water to rainfall (“autoconversion”) that can be used within large-scale climate models, and evaluates the new method using the Regional Climate Model, version 3 (RegCM3), coupled to the land surface scheme Integrated Biosphere Simulator (IBIS). The new method is derived from observed distributions of cloud water content and is constrained by observations of cloud droplet characteristics and climatological rainfall intensity. This new method explicitly accounts for subgrid variability with respect to cloud water density and is independent of model resolution, making it generally applicable for large-scale climate models. This work builds on the development of a new parameterization method for convective cloud fraction, which was described in Part I.

Simulations over the Maritime Continent using the Emanuel convection scheme show significant improvement in model performance, not only with respect to convective rainfall but also in shortwave radiation, net radiation, and turbulent surface fluxes of latent and sensible heat, without any additional modifications made to the simulation of those variables. Model improvements are demonstrated over a 19-yr validation period as well as a shorter 4-yr evaluation. Model performance with the Grell convection scheme is not similarly improved and reasons for this outcome are discussed. This work illustrates the importance of representing observed subgrid-scale variability in diurnally varying convective processes for simulations of the Maritime Continent region.

1. Introduction

The skill of large-scale climate models in reproducing the existing climate has improved significantly over many parts of the world, but simulations over the Maritime Continent region still contain substantial error (e.g., Yang and Slingo 2001; Neale and Slingo 2003; Dai and Trenberth 2004; Wang et al. 2007). Gianotti et al. (2012) showed that the Regional Climate Model, version 3.0 (RegCM3), coupled with the land surface scheme Integrated Biosphere Simulator (IBIS) also exhibited significant error over the Maritime Continent region with respect to rainfall, net radiation, latent and sensible heat fluxes, and evapotranspiration over the land surface. These errors are not unique but are consistent with other published climate modeling studies over the Maritime Continent region (e.g., Chow et al. 2006; Francisco et al. 2006; Martin et al. 2006; Wang et al. 2007). It was argued that the source of these errors resided primarily in the

atmospheric component (i.e., RegCM3) of the coupled model system, specifically with the simulation of convective cloud and rainfall processes (Gianotti et al. 2012).

In the Intergovernmental Panel on Climate Change Fourth Assessment Report (IPCC AR4), cloud feedbacks were identified as a primary reason for differences between models, with the shortwave impact of boundary layer and midlevel clouds making the largest contribution (Christensen et al. 2007). Of the wide range of time scales exhibited by clouds, variability on the diurnal scale is particularly important since it influences diurnal energetics of the atmosphere and surface (Bergman and Salby 1996). However, it was shown in Gianotti (2012) and Gianotti and Eltahir (2014, hereafter Part I) that the default parameterization of convective cloud fraction in RegCM3 did not simulate a reasonable diurnally varying convective–radiative feedback. This issue was addressed in Part I by introducing a new method for parameterizing convective cloud fraction.

However, the formation of convective clouds represents only one part of the diurnal cycle of convective cloud activity. The production of convective rainfall is a significant cloud dissipation mechanism in climate

Corresponding author address: Rebecca L. Gianotti, MIT Room 48-207, 15 Vassar Street, Cambridge, MA 02139.
E-mail: rlg@alum.mit.edu

models and therefore is a critical component of convective cloud simulation. Most GCMs and RCMs use one or more associated equations to parameterize the suite of processes responsible for precipitation production, which is termed “autoconversion.”

This work describes a new parameterization method for convective autoconversion and its implementation within RegCM3-IBIS. The new method explicitly accounts for subgrid variability in rainfall production and is independent of model resolution, making it generally applicable for use in large-scale climate models.

2. Parameterization methods for convective autoconversion

a. Commonly used methods in large-scale climate models

Global and regional climate models (GCMs and RCMs) usually employ bulk microphysics schemes in which the hydrometeor representation is reduced to two variables—cloud droplets and precipitating particles—that are characterized by their mixing ratios (Geoffroy et al. 2008). Hence most autoconversion parameterization methods relate rainfall production to some dependence on cloud liquid water. Arguably the most commonly used of these methods are those developed by Kessler (1969), Arakawa and Schubert (1974), and Sundqvist et al. (1989).

In the scheme developed by Kessler (1969), the efficiency of autoconversion increases linearly with cloud water content but is zero below some threshold, that is,

$$\frac{dM}{dt} = k_1(m - a) \begin{cases} k_1 > 0 & \text{when } m > a \\ k_1 = 0 & \text{when } m < a \end{cases} \quad (1)$$

where M is the rainwater mixing ratio, m is the cloud liquid water (CLW) mixing ratio, $k_1 = 10^{-3} \text{ s}^{-1}$, and a is a CLW threshold value below which cloud conversion does not occur. Kessler (1969) noted that a reasonable threshold value would be 1 g m^{-3} . This form of autoconversion was implemented in the Colorado State University GCM (Fowler et al. 1996) and in the fifth-generation Pennsylvania State University–National Center for Atmospheric Research Mesoscale Model (MM5; Grell et al. 1994), as well as in the cloud-resolving model System for Atmospheric Modeling, version 6.3 (SAM 6.3; Khairoutdinov and Randall 2003).

Arakawa and Schubert (1974) used the following parameterization for the rainfall rate out of a subensemble of cumulus clouds at a given elevation z :

$$r(z) = C_0 l(z), \quad (2)$$

where C_0 is a constant parameter and $l(z)$ is the mixing ratio of CLW.

Lord (1982) proposed a similar autoconversion function that includes a dependence on the vertical flux of cloud water in the updraft, where $C_0 = 0.002 \text{ m}^{-1}$. This is the form of autoconversion is used within the Community Atmosphere Model, version 4.0 (CAM4.0; Neale et al. 2010).

In the model described by Sundqvist et al. (1989), the rate of release of both convective and stratiform precipitation is given by

$$P = c_0 m \left\{ 1 - \exp \left[- \left(\frac{m}{b m_r} \right)^2 \right] \right\}, \quad (3)$$

where $1/c_0$ is the characteristic time scale for the conversion of cloud droplets into raindrops, b is cloud cover, m_r the within-cloud threshold value for cloud water, and m the gridcell value of cloud water (hence m/b is the within-cloud value of cloud water). The parameter m_r is assigned a value typical of individual cloud types, which is invariant to grid resolution. The values of c_0 and m_r are modified by temperature to account for the more rapid autoconversion processes involving ice. This method of autoconversion was adopted by Tiedtke (1993) and is used in the National Aeronautics and Space Administration (NASA) Goddard Institute for Space Studies (GISS) GCM (Del Genio et al. 1996).

Some large-scale climate models also include prognostic droplet size and concentration variables. Those models may use autoconversion parameterizations based on the method of Manton and Cotton (1977), which depends on the mean concentration, radius, and collision frequency of cloud water droplets. Once the critical droplet radius r_{crit} is prescribed and the cloud droplet number concentration N_d is known at a grid point, the threshold cloud liquid-water mixing ratio below which no autoconversion occurs can be estimated. While this method is more sophisticated than others, many models do not include droplet concentration and radius as prognostic variables.

The major drawback of all these autoconversion methods is the lack of subgrid variability in cloud water content and rainfall production. The methods rely on grid-mean values of the simulated variables and thresholds, and therefore rainfall is produced uniformly over a model grid cell.

GCM and RCM simulations can exhibit strong sensitivity to the parameters controlling autoconversion. For models that use a critical cloud water mixing ratio threshold, it is common to use a value considerably smaller than the within-cloud value of about 1 g kg^{-1} suggested by Kessler (1969). For example, the Met Office

Unified Model uses a threshold of 0.2 g kg^{-1} , the Colorado State University GCM uses 0.25 g kg^{-1} , the NASA GISS GCM uses 0.5 g m^{-3} , and the Scripps Institution of Oceanography GCM uses 0.3 g kg^{-1} (Xu et al. 2005). The cloud-resolving model SAM 6.3 employs a threshold of 1 g kg^{-1} (Blossey et al. 2007) because it runs at a scale sufficiently small (with a horizontal resolution on the order of 1 km) to resolve the natural variability in convective activity. For models that have a prognostic droplet radius and concentration, observations suggest that the critical drop size radius is $10\text{--}15 \mu\text{m}$, but GCMs typically use $4.5\text{--}7.5 \mu\text{m}$ in order to get good simulated values of cloud liquid water (Rotstajn 2000; Geoffroy et al. 2008).

These lower, tuned parameter values could be interpreted as grid-mean thresholds and therefore comparable to the grid-mean simulated condensate. But because these thresholds are not functions of the actual subgrid variability in condensate, they must be manually tuned to account for different model resolutions, domains, and choice of parameterization schemes. Their use is therefore less than ideal.

Rotstajn (2000) added a new treatment of stratiform clouds to the Commonwealth Scientific and Industrial Research Organisation (CSIRO) GCM to simulate the subgrid-scale variability in stratiform autoconversion. The assumed subgrid moisture distribution from the model's condensation scheme was applied in each grid box to determine the fraction of the cloudy area in which the mean within-cloud mixing ratio exceeded a prescribed threshold, and autoconversion occurred only in that fraction of the grid cell (Rotstajn 2000). The total water mixing ratio was assumed to follow a symmetric triangular probability density function (PDF) about its grid-mean value. This method allowed the critical value of the threshold droplet radius to increase from $7.5 \mu\text{m}$ in the old treatment to $9.3 \mu\text{m}$ in the new treatment, close to observations (Rotstajn 2000). This scheme improves the representation of subgrid-scale variability in autoconversion. But it requires a prognostic droplet concentration variable, which is not always available in large-scale climate models, and employs a somewhat arbitrary symmetric triangular PDF to describe the total water mixing ratio.

b. Existing parameterization of convective autoconversion within RegCM3

The Grell convective parameterization scheme available within RegCM3 uses a method based on Arakawa and Schubert (1974) to calculate the convective rainfall produced at a given elevation, $R(z)$:

$$R(z) = \frac{c_0 \Delta z}{1 + c_0 \Delta z} (q_u - q_{\text{rch}}) M_u, \quad (4)$$

where c_0 is 0.002, Δz is the depth of model layer, q_u is the water vapor mixing ratio of updraft, q_{rch} is the water vapor mixing ratio of environment, and M_u is updraft mass flux. The quantity shown in parentheses is equivalent to the grid-mean CLW for that model layer.

Since there is no discussion of this formulation in Grell (1993) or the RegCM3 manual, it is assumed that the value of c_0 is taken from Lord (1982). Because the vertical model layers are defined within RegCM3 to be thinner in the lower atmosphere and increase in thickness with increasing height above the surface, this autoconversion function results in a minimum efficiency of about 0.5 in the lower atmosphere and a maximum efficiency of about 0.8 at high altitudes.

The Emanuel scheme within RegCM3 uses a Kessler form of autoconversion to calculate the production of convective rainfall at a given elevation, $R(z)$:

$$R(z) = \overline{\text{CLW}}(z) - \text{CLW}_T, \quad (5)$$

where $\overline{\text{CLW}}(z)$ is grid-scale CLW within model layer z , and CLW_T is the threshold value of CLW. By default, $\text{CLW}_T = 1.1 \text{ g kg}^{-1}$.

The default threshold value is close to observed values of cloud density. However, it represents a point-scale threshold value, while the grid-mean cloud water mixing ratio $\overline{\text{CLW}}$ is used to calculate simulated rainfall. Hence there is a mismatch of scales in this formulation within RegCM3. In the work presented in Gianotti (2012) and Part I, the threshold was set to 0.25 g kg^{-1} to attempt a better matching of scales, but that kind of tuning should ideally be avoided.

3. New parameterization method for convective autoconversion

A new method has been developed to parameterize convective autoconversion. This method is in the spirit of the semiempirical approach described by Emanuel (1994), in which physical principles are used to constrain a system to a limited number of parameters, whose values are then related to observations.

As a first-order approximation, the long-term average efficiency of convective rainfall production is considered constant. Empirical relationships are then used to frame an expression for the time-mean autoconversion, as follows. When nonzero rainfall is simulated within a model grid cell, the fractional area of the grid cell that contains rainfall can be estimated using the relationship derived by Eltahir and Bras (1993):

$$\mu = \frac{\overline{R}}{R_{\text{clim}}}, \quad (6)$$

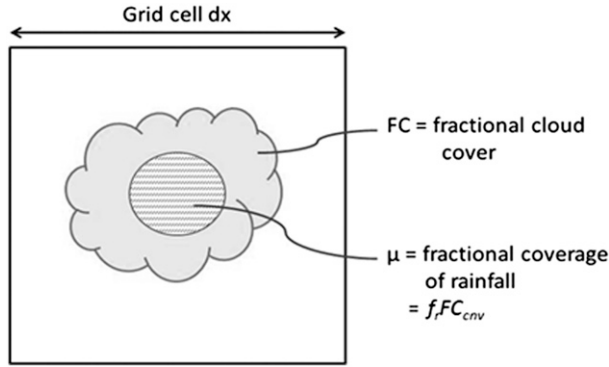


FIG. 1. Relationship between fractional cloud cover FC and fractional coverage of rainfall μ .

where μ is the fractional coverage of rainfall, \bar{R} is the grid-average simulated rainfall and R_{clim} is the climatological rainfall intensity, which is the average rainfall intensity observed when there is nonnegligible rainfall. The fractional coverage of rainfall within a raining model grid cell may also be expressed as the portion of the cloudy area within a grid cell that produces rainfall:

$$\mu = f_r FC_{\text{cnv}}, \quad (7)$$

where f_r is the fraction of total cloudy area that is raining and FC_{cnv} is the fractional coverage of convective cloud. This relationship is illustrated schematically in Fig. 1.

A new method for parameterizing convective cloud fraction is described by (Gianotti 2012; Part I)

$$FC_{\text{cnv}} = \frac{\overline{\text{CLW}}}{\text{CLW}_{\text{clim}}}, \quad (8)$$

where $\overline{\text{CLW}}$ is the simulated grid-average value of CLW and CLW_{clim} is the climatological cloud liquid water density (i.e., the mean observed cloud water content).

Combining the two expressions for the fractional coverage of rainfall yields

$$\frac{\bar{R}}{R_{\text{clim}}} = f_r \frac{\overline{\text{CLW}}}{\text{CLW}_{\text{clim}}}. \quad (9)$$

The simulated grid-average rainfall can be represented as some fraction f_e of the simulated CLW, that is,

$$\bar{R} = f_e \overline{\text{CLW}}, \quad (10)$$

where f_e is the autoconversion efficiency, which can be expressed as

$$f_e = f_r \frac{R_{\text{clim}}}{\text{CLW}_{\text{clim}}}. \quad (11)$$

The form of f_r is now required. In the physical world, if CLW is distributed according to a PDF, then the quantity f_r is equivalent to the portion of that PDF that exceeds some threshold for autoconversion, CLW_T , that is,

$$f_r = \int_{\text{CLW}_T}^{\infty} f_{\text{CLW}} d\text{CLW}. \quad (12)$$

The observed distribution of CLW has been fitted to a lognormal distribution (Foster et al. 2006) and a Weibull distribution (Iassamen et al. 2009). Rainfall drop size distributions have been fitted to exponential (Marshall and Palmer 1948), lognormal (Rosenfeld and Ulbrich 2003), and gamma (Ulbrich 1983; Testud et al. 2001) distributions. For simplicity and in the absence of a well-defined PDF for CLW, an exponential distribution of CLW is used here (noting that other distributions may collapse to the exponential distribution with appropriate parameter choices). It should also be noted that a lognormal distribution for CLW was attempted in this work but no significant differences from an exponential distribution were found in the results. The exponential distribution is also advantageous since it can be integrated analytically a priori, increasing computational efficiency.

If the observed CLW is distributed exponentially with a mean of CLW_{clim} , then

$$\begin{aligned} f_r &= \int_{\text{CLW}_T}^{\infty} \frac{1}{\text{CLW}_{\text{clim}}} \exp\left(-\frac{\text{CLW}}{\text{CLW}_{\text{clim}}}\right) d\text{CLW} \\ &= \exp\left(-\frac{\text{CLW}_T}{\text{CLW}_{\text{clim}}}\right), \end{aligned} \quad (13)$$

which results in

$$f_e = \exp\left(-\frac{\text{CLW}_T}{\text{CLW}_{\text{clim}}}\right) \frac{R_{\text{clim}}}{\text{CLW}_{\text{clim}}}. \quad (14)$$

This relationship represents the long-term mean climatological rainfall production efficiency, as shown in Fig. 2. However, at the point scale the autoconversion efficiency will be dynamic and spatially variable. It is desirable to capture this temporal and spatial variability within a model to improve the physical realism of the simulation. To achieve this, a point-scale expression for autoconversion can be used to derive an instantaneous autoconversion efficiency that accounts for the impact of subgrid-scale variability.

At the scale of a small parcel of convective cloud, the volume of rainfall will be a function of the cloud droplets that are large enough to fall, which can be represented as

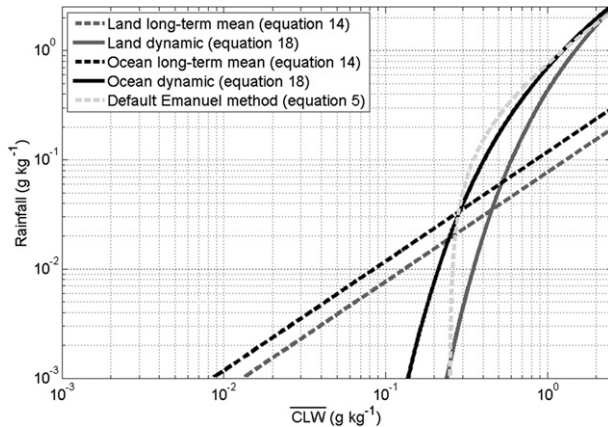


FIG. 2. Relationship between simulated grid-mean $\overline{\text{CLW}}$ (g kg^{-1}) and simulated grid-scale rainfall (g kg^{-1}) calculated using the long-term mean autoconversion efficiency [Eq. (14)] compared to the instantaneous dynamic autoconversion efficiency [Eq. (18)], developed using typical values for land and ocean provided by observations (see Table 2). Note the log-log axes. Also shown for comparison is the default version of autoconversion within the Emanuel convection scheme in RegCM3 [Eq. (5)], using a threshold value of $\text{CLW}_T = 0.25 \text{ g kg}^{-1}$.

$$R = \alpha(\text{CLW} - \text{CLW}_T)^n \quad \text{for } \text{CLW} > \text{CLW}_T, \quad (15)$$

where R is point-scale rainfall, CLW is the amount of CLW within the cloud parcel, CLW_T is the point-scale threshold of CLW that must be exceeded to produce rainfall, and n is the parameter that represents the degree of linearity of the autoconversion process. The coefficient α (it is assumed that $\alpha = 1$) ensures that the units remain dimensionally consistent for cases when $n \neq 1$.

This point-scale relationship follows the Kessler form and would duplicate the Kessler method if $n = 1$. However, the generalized form in which $n \neq 1$ accounts for the many complexities involved in converting cloud droplets to rainfall, such as the effects of turbulent mixing and variability in cloud condensation nuclei size and abundance. Such nonlinear processes have been proposed as explanations for the difference between theory and observations of rainfall production (Emanuel 1994; Khain et al. 2000; Stephens and Haynes 2007).

If the convective CLW within a model grid cell is distributed with the PDF f_{CLW} , then \bar{R} can be written as

$$\bar{R} = \alpha \int_{\text{CLW}_T}^{\infty} (\text{CLW} - \text{CLW}_T)^n f_{\text{CLW}} d\text{CLW}. \quad (16)$$

Within a model grid cell, if the simulated distribution of convective CLW f_{CLW} is also assumed to follow an exponential distribution with a mean value of $\overline{\text{CLW}}$ (the simulated instantaneous grid-mean value of CLW), then

$$\bar{R} = \alpha \overline{\text{CLW}}^n \Gamma(n+1) \exp\left(-\frac{\text{CLW}_T}{\overline{\text{CLW}}}\right), \quad (17)$$

where Γ is the gamma function, which can be evaluated via lookup tables.

This expression can now be used to derive a dynamic, grid-scale measure of the autoconversion efficiency:

$$f_e = \alpha \overline{\text{CLW}}^{n-1} \Gamma(n+1) \exp\left(-\frac{\text{CLW}_T}{\overline{\text{CLW}}}\right). \quad (18)$$

This function requires specification of two parameter values: CLW_T and n , assuming $\alpha = 1$. It is desirable to have these values constrained by observations. Unfortunately, observations of CLW are limited to non-precipitating retrievals and hence there are no direct observations of autoconversion. But observations have been made of the radius required for a cloud droplet to convert into a precipitating raindrop and of the droplet number concentration at the time that the critical threshold radius is breached. An approximate value of CLW_T can be estimated from these observations, as follows:

$$\text{CLW}_T = \frac{4}{3} \pi \rho N_{d,\text{crit}} r_{\text{crit}}^3, \quad (19)$$

where CLW_T is threshold cloud water content (g m^{-3}), ρ is liquid water density (g m^{-3}), $N_{d,\text{crit}}$ is droplet concentration corresponding to critical radius (m^{-3}), and r_{crit} is the critical radius for rainfall formation of cloud droplets (m).

Table 1 lists observations of the critical droplet radius and droplet concentration in continental and maritime clouds. Since the islands in the Maritime Continent often experience biomass burning, it seems reasonable to adopt $r_{\text{crit}} \approx 8 \mu\text{m}$ and $N_d \approx 700 \text{ cm}^{-3}$. Using these values in Eq. (19) leads to $\text{CLW}_{T,\text{land}} \approx 1.5 \text{ g m}^{-3}$. Over ocean, it seems reasonable to adopt $r_{\text{crit}} \approx 14 \mu\text{m}$ and $N_d \approx 60 \text{ cm}^{-3}$. This leads to $\text{CLW}_{T,\text{ocean}} \approx 0.7 \text{ g m}^{-3}$. But it also seems sensible to set $\text{CLW}_T > \text{CLW}_{\text{clim}}$, since the average observed cloud density is likely to be nonprecipitating. Given that the observed value of $\text{CLW}_{\text{clim,ocean}} \approx 0.7 \text{ g m}^{-3}$ (Table 1), it seems reasonable to set $\text{CLW}_{T,\text{ocean}} \approx 0.75 \text{ g m}^{-3}$.

It now remains to evaluate the parameter n , which could be attempted in multiple ways. One method is to constrain the instantaneous autoconversion efficiency by the long-term mean efficiency. This requires values for R_{clim} and CLW_{clim} .

Data from Singapore's Changi airport meteorological station (described in Gianotti et al. 2012), the Tropical Rainfall Measuring Mission (TRMM)'s 3B42 product (described in section 4), and Table 1 of Eltahir and Bras

TABLE 1. Observations used to constrain new autoconversion function.

Cumulus cloud type	Quantity	Value	Reference
Continental, general	Liquid water content	0.1–3 g m ⁻³	Rosenfeld and Lensky (1998)
	Liquid water content	1 g m ⁻³	Rogers and Yau (1989)
	Critical droplet radius, r_{crit}	9–10 μm	Brenguier et al. (2000)
	Droplet concentration, N_d	Median = 228 cm ⁻³ , third quartile = 310 cm ⁻³	Squires (1958)
Continental, biomass burning	Critical droplet radius, r_{crit}	3–8 μm	Reid et al. (1999)
	Critical droplet concentration, N_d	3000 cm ⁻³	Reid et al. (1999)
Maritime	Liquid water content	0.25–1.3 g m ⁻³	Rangno and Hobbs (2005)
	Liquid water content	0.4–1.2 g m ⁻³	Warner (1955)
	Critical droplet radius, r_{crit}	15 μm	Kubar et al. (2009)
	Critical droplet radius, r_{crit}	12–15 μm	Rangno and Hobbs (2005)
	Critical droplet radius, r_{crit}	13–14 μm	Brenguier et al. (2000)
	Critical droplet concentration, N_d	60 cm ⁻³	Kubar et al. (2009)
	Critical droplet concentration, N_d	70 cm ⁻³	Rangno and Hobbs (2005)
	Droplet concentration, N_d	Median = 45 cm ⁻³	Squires (1958)

(1993) suggest $R_{\text{clim,land}} \approx 4.85 \text{ mm h}^{-1}$ and $R_{\text{clim,ocean}} \approx 3.5 \text{ mm h}^{-1}$ for the Maritime Continent.

To provide a direct comparison between CLW and rainfall, the climatological rainfall rates R_{clim} (mm h^{-1}) can be converted to mixing ratios (i.e., the mass of rainfall falling through a unit volume of air), by assuming an exponential size distribution for raindrops as in Marshall and Palmer (1948) and by using the functions provided by Rosenfeld and Ulbrich (2003). These yield $R_{\text{clim,land}} = 0.32 \text{ g m}^{-3} \text{ h}^{-1}$ and $R_{\text{clim,ocean}} = 0.24 \text{ g m}^{-3} \text{ h}^{-1}$.

The data presented in Table 1 suggest that $\text{CLW}_{\text{clim,land}} \approx 1.2 \text{ g m}^{-3}$ and $\text{CLW}_{\text{clim,ocean}} \approx 0.7 \text{ g m}^{-3}$. Using these values in Eq. (14) leads to a mean autoconversion efficiency of $f_e \approx 0.1$ over both land and ocean.

Values of the simulated grid-scale $\overline{\text{CLW}}$ are now required to evaluate the dynamic autoconversion efficiency using Eq. (18). With both the Grell and Emanuel convection schemes in RegCM3, typical instantaneous values of $\overline{\text{CLW}}$ were approximately 0.5 g m^{-3} over land and 0.3 g m^{-3} over ocean. Model output is not shown for brevity. Using these values in Eq. (18) leads to $n = 0.9$ over land and $n = 0.94$ over ocean.

Another possible way to constrain parameter n is to set the efficiency equal to 1 at some upper threshold value for $\overline{\text{CLW}}$. It is noted that the same parameter values of $n = 0.9$ over land and $n = 0.94$ over ocean can be derived by assuming that $f_e = 1$ when $\overline{\text{CLW}} = 2.5 \text{ g m}^{-3}$ over land and 2 g m^{-3} over ocean, close to the highest observed values of CLW (see Table 1).

Hence the following expressions are obtained for the grid-mean convective rainfall:

$$\bar{R} = \overline{\text{CLW}}^{0.9} 0.9618 \exp\left(-\frac{0.0015}{\overline{\text{CLW}}}\right) \text{ for land} \quad (20a)$$

and

$$\bar{R} = \overline{\text{CLW}}^{0.94} 0.9761 \exp\left(-\frac{0.00075}{\overline{\text{CLW}}}\right) \text{ for ocean,} \quad (20b)$$

where $\overline{\text{CLW}}$ is the simulated grid-mean CLW (kg kg^{-1}). These relationships are illustrated in Fig. 2. The figure shows that rainfall production using the dynamic method is much more efficient than the long-term mean autoconversion efficiency for high $\overline{\text{CLW}}$ values but less efficient at low $\overline{\text{CLW}}$ values.

RegCM3 uses only a single prognostic variable, liquid water mixing ratio, but in reality the autoconversion efficiency is strongly dependent upon the type of hydrometeor. In particular, the conversion of cloud ice crystals to precipitation is known to be much faster than the conversion of cloud liquid droplets (Rogers and Yau 1989). To account for this difference, the Emanuel convection scheme scales CLW_T in temperatures below a certain threshold, as follows:

$$\text{CLW}_{T,\text{actual}} = \text{CLW}_T \text{ for } T \geq 0^\circ\text{C}, \quad (21a)$$

$$\begin{aligned} &\text{CLW}_{T,\text{actual}} \\ &= \text{CLW}_T \left(1 - \frac{T}{-55^\circ\text{C}}\right) \text{ for } -55^\circ\text{C} \leq T \leq 0^\circ\text{C}, \end{aligned} \quad (21b)$$

and

$$\text{CLW}_{T,\text{actual}} = 0 \text{ for } T \leq -55^\circ\text{C}. \quad (21c)$$

This increases the autoconversion efficiency in cold clouds where ice crystals would be expected to dominate. This same scaling is included in the new autoconversion method presented here, but a detailed treatment of

TABLE 2. Values of parameters used in derivation of new convective autoconversion parameterization.

Parameter	Land	Ocean	Notes
R_{clim}	4.85 mm h ⁻¹ , 0.32 g m ⁻³ h ⁻¹	3.5 mm h ⁻¹ , 0.24 g m ⁻³ h ⁻¹	Data from Changi airport, Singapore (Gianotti et al. 2012), TRMM 3B42 product (see section 3c) (Table 1 of Eltahir and Bras 1993). Unit conversion used functions from Marshall and Palmer (1948) and Rosenfeld and Ulbrich (2003).
CLW_{clim}	1.2 g m ⁻³	0.7 g m ⁻³	Estimated from observations in Rangno and Hobbs (2005), Rogers and Yau (1989), Rosenfeld and Lensky (1998), and Warner (1955).
CLW_T	1.5 g m ⁻³	0.75 g m ⁻³	Derived from observations in Brenguier et al. (2000), Kubar et al. (2009), Rangno and Hobbs (2005), Reid et al. (1999), and Squires (1958).
n	0.94	0.9	Derived by matching instantaneous autoconversion efficiency to long-term mean efficiency.
$\overline{\text{CLW}}$	2.5 g m ⁻³	2 g m ⁻³	Taken from model output (not shown).

ice-phase precipitation should be a priority for future work.

Table 2 summarizes the parameter values used in this derivation. However, it is noted that these values are chosen from within ranges of observed values (Table 1). Therefore it would be reasonable for the model user to choose parameter values within these ranges to explore the impact of different parameter choices on model performance.

It is noted that if a value of $n = 1$ is assumed with the new formulation, and the corresponding value of CLW_T is derived using observed values of R_{clim} and CLW_{clim} for the Maritime Continent region, a value of $\text{CLW}_T \simeq 0.3 \text{ g m}^{-3}$ is obtained. This is similar to the “tuned” values of CLW_T used in some GCMs including that used in Part I. Indeed, Fig. 2 shows the similarity between the dynamic autoconversion and the tuned version of the default Emanuel method. The generalized form presented here, where $n = 1$ is not assumed a priori, removes the need to tune a grid-mean value.

The new formulation for autoconversion presented here has significant advantages over the default forms that exist within RegCM3: 1) it explicitly recognizes subgrid variability in CLW and how that variability affects the grid-scale conversion process; 2) only two parameters have to be specified, one dependent upon the other, which are constrained by observations; and 3) it can be applied consistently across convection schemes, bringing added realism to a model independently of user choices.

4. Simulations using the new convective autoconversion parameterization

a. Model description

This work uses RegCM3–IBIS as described in Gianotti et al. (2012), including the subgrid explicit moisture SUBEX scheme (Pal et al. 2000) for resolvable,

large-scale clouds and precipitation, the choice of Grell (Grell 1993) with Fritsch–Chappell (F-C; Fritsch and Chappell 1980) or Arakawa–Schubert (Grell et al. 1994) closures, and Emanuel (Emanuel 1991; Emanuel and Živković–Rothman 1999) convective parameterization schemes. Further details of the developments and description of RegCM3 are available in Pal et al. (2007).

Giorgi et al. (2012) describes upgrades that were incorporated into the more recent version RegCM, version 4 (RegCM4), which was made publicly available in 2011. RegCM4 does not contain any upgrades to convective parameterization relevant to this work.

Some modifications were made to the boundary layer parameterization scheme (Holtslag et al. 1990; Holtslag and Boville 1993) within RegCM3, the simulation of large-scale clouds within the PBL, soil thermal conductivity, and ocean surface roughness (see Gianotti 2012 for details). The vertical limit on simulated cloud cover was also extended to permit clouds up to an altitude of about 16 km. The combination of these modifications resulted in small reductions to the land and ocean surface latent heat fluxes, a substantial reduction in the PBL height, removing an overestimation bias in the PBL height over land at night, and removal of egregious nighttime low-level large-scale clouds over land (Gianotti 2012). However, none of these modifications significantly impacted the simulation of radiative fluxes or rainfall.

b. Experimental design

Two sets of simulations were run to evaluate the performance of the new autoconversion parameterization within RegCM3–IBIS. In all simulations described below, the new parameterization was implemented as follows.

Both the Grell and Emanuel convection schemes in RegCM3 simulate rainfall within a model layer using a function of the form shown in Eq. (10), that is, as the product of some autoconversion efficiency and the

grid-mean CLW within that layer. In the Grell scheme, the efficiency is a function of the grid-mean updraft mass flux M_u and two constant parameters (model layer thickness and a coefficient). Note that the quantity shown in parentheses in Eq. (4) is equivalent to the grid-mean CLW. In the Emanuel scheme, the efficiency is a function of the CLW threshold, CLW_T . Hence in both convection schemes, the new autoconversion efficiency function shown in Eq. (18) simply replaces the existing efficiency function such that the rainfall calculation remains of the form shown in Eq. (10). Since both convection schemes calculate the amount of condensate (i.e., CLW) resulting from the grid-mean water vapor mixing ratio and saturation vapor pressure, the new autoconversion parameterization can be implemented consistently across convection schemes.

The first simulations were shorter and were used to evaluate the impact of the new autoconversion method relative to other model modifications made by these authors. Included in this set are simulations in which the planetary boundary layer region has been modified as described above [labeled Mod; see Gianotti (2012) for details], simulations incorporating both boundary layer modifications and the new parameterization of convective cloud fraction shown in Eq. (8) (labeled New; see Part I for details), and simulations combining the new convective autoconversion with all other modifications (labeled Auto). Simulations began on 1 July 1997 and ended 31 December 2001. The first 6 months of output were ignored to allow for spinup. The remaining 4 years of simulation (1998–2001) were used for evaluation of model performance.

A second set of two simulations was run to validate the performance of the newly modified RegCM3–IBIS over a longer time period. One simulation uses the default version of RegCM3–IBIS [labeled Def; for details see Gianotti et al. (2012)]; the other simulation incorporates all the model modifications mentioned here (i.e., as in Auto). These simulations used the Emanuel

TABLE 3. List of parameters used in SUBEX and their default values (based on Pal et al. 2000).

Parameter	Land	Ocean
Cloud formation threshold RH_{\min}	0.8	0.9
Maximum saturation RH_{\max}	1.01	1.01
Autoconversion rate C_{ppt} (s^{-1})	5×10^{-4}	5×10^{-4}
Autoconversion scale factor C_{acs}	0.65	0.3
Accretion rate C_{acc} ($m^3 kg^{-1} s^{-1}$)	6	6
Raindrop evaporation rate C_{evap} [$(kg m^{-2} s^{-1})^{-1/2} s^{-1}$]	2×10^{-5}	2×10^{-5}

convection scheme, beginning on 1 July 1982 and ending 31 December 2001. The first 6 months of output were ignored to allow for spinup. The remaining 19 years of simulation (1983–2001) were used for model evaluation. These years were chosen so that the same datasets could be used for lateral boundary conditions as for the 4-yr simulations, with similar observational datasets, for consistency.

Table 3 presents the parameter values used in the SUBEX routine in this study. The default values were based on the original version of the scheme, as described in Pal et al. (2000). It should be noted that although the large-scale SUBEX routine and the convective parameterization schemes operate independently within the RegCM3 structure, each routine can significantly impact the other by altering grid-scale variables such as temperature and water vapor. Therefore the model user should be cognizant of how changes introduced to the large-scale scheme affect convection, including the impact of the new parameterization presented here, and vice versa.

For all simulations, the model domain (Fig. 3) was centered along the equator at $115^\circ E$, used a normal Mercator projection, and spanned 95 grid points meridionally and 200 grid points zonally, with a horizontal resolution of 30 km. The simulations used 18 vertical sigma levels, from the ground surface up to the 50-mb level. The land surface scheme was run every 120 s, twice the model time step.

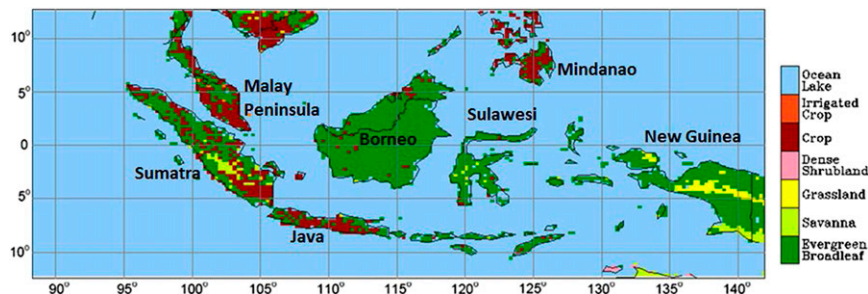


FIG. 3. Model domain showing vegetation classification used for IBIS. The domain has been sized such that it covers the generally accepted extent of the Maritime Continent region. Major islands are labeled.

TABLE 4. Varying characteristics of simulations used in study. The names are used to reference each simulation in the text.

Simulation name	Convection scheme	Modified PBL region*	Convective cloud fraction	Convective autoconversion	Evaluation period
GFC-Mod	Grell with F-C	Yes	Default	Default	1998–2001
GFC-New	Grell with F-C	Yes	New**	Default	1998–2001
GFC-Auto	Grell with F-C	Yes	New**	New	1998–2001
EMAN-Mod	Emanuel	Yes	Default	Default	1998–2001
EMAN-New	Emanuel	Yes	New**	Default	1998–2001
EMAN-Auto	Emanuel	Yes	New**	New	1998–2001
EMAN-Def_Long	Emanuel	No	Default	Default	1983–2001
EMAN-Auto_Long	Emanuel	Yes	New**	New	1983–2001

* Refers to simulation of PBL height, ocean surface roughness, soil heat flux, and large-scale clouds within the PBL region, as described in Gianotti (2012).

** As described in Gianotti (2012) and Part I.

Sea surface temperatures (SSTs) were prescribed using the National Ocean and Atmospheric Administration (NOAA) optimally interpolated SST (OISST) dataset, which is available at $1^\circ \times 1^\circ$ resolution and at a weekly time scale beginning in 1982 (Reynolds et al. 2002). Topographic information was taken from the United States Geological Survey's Global 30-arc-s elevation dataset (GTOPO30), aggregated to 10 arc min (United States Geological Survey 1996). Vegetation biomes were based on the potential global vegetation dataset of Ramankutty (1999), modified to include two extra biomes for inland water and ocean as described in Winter et al. (2009). In all simulations presented, RegCM3-IBIS was run only with static vegetation.

Soil properties, including albedo and porosity, were determined based on the relative proportions of clay and sand in each grid cell. Sand and clay percentages were taken from the Global Soil Dataset, which has a spatial resolution of 5 min (Global Soil Data Task, IGDP-DIS 2000). Soil moisture, temperature, and ice content were initialized using the output from a global $0.5^\circ \times 0.5^\circ$ resolution 20-yr offline simulation of IBIS as described in Winter et al. (2009).

The 40-yr European Centre for Medium-Range Weather Forecasts (ECMWF) Re-Analysis (ERA-40) dataset, available from September 1957 to August 2002 (Uppala et al. 2005), was used to force the boundaries in all simulations. The exponential relaxation technique of Davies and Turner (1977) was used with both datasets.

Eight simulations in total are presented in this study. Table 4 summarizes the different characteristics of these simulations and lists the names used to reference each simulation throughout the text.

c. Comparison datasets

Solar radiation is compared to the NASA/Global Energy and Water Cycle Experiment (GEWEX) Surface Radiation Budget (SRB) dataset release 3.0 (Stackhouse

et al. 2011), made available by the NASA Langley Research Center Atmospheric Sciences Data Center. SRB is available at 3-hourly intervals from 1983 onward on a $1^\circ \times 1^\circ$ global grid. Data were interpolated to the model domain for direct comparison.

Observations of latent heat flux over land are taken from field studies of evapotranspiration (ET) in the Maritime Continent, as described in Table 4 of Gianotti et al. (2012). For all simulations, it is assumed that the fluxes measured by these field studies apply over the entire evaluation period. Over ocean, latent and sensible heat flux observations are from the Woods Hole Oceanographic Institution (WHOI) global dataset of ocean evaporation (Yu et al. 2008), which is available from 1958 onward on a $1^\circ \times 1^\circ$ global grid.

Rainfall from the 4-yr simulations is compared to the TRMM Multisatellite Precipitation Analysis (TMPA) $0.25^\circ \times 0.25^\circ$ resolution 3B42 product (described in Huffman et al. 2007), available from 1998 onward and referenced in this work simply as TRMM. Relative proportions of convective and large-scale rain are taken from Mori et al. (2004), who used the 2A25, 2A12, and 2B31 TRMM products to describe the climatological convective versus stratiform rainfall split over Indonesia.

Total rainfall from the 19-yr simulations is compared to the Global Precipitation Climatology Project (GPCP) version 2.2 combined precipitation dataset, available at monthly resolution from 1979 to the present on a $2.5^\circ \times 2.5^\circ$ global grid (Adler et al. 2003). GPCP data are provided by the NOAA Office of Oceanic and Atmospheric Research/Earth System Research Laboratory Physical Sciences Division (NOAA/OAR/ESRL PSD) from their website (<http://www.esrl.noaa.gov/psd/>). It is assumed that the convective and large-scale rainfall fractions obtained from the TRMM data also apply over the 19-yr evaluation period; these fractions are used to separate the total rainfall from GPCP into convective and large-scale components.

Fractional cloud cover from the 4-yr simulations is compared to the International Satellite Cloud Climatology Project (ISCCP) stage D2 product (Rossow et al. 1996), made available by NASA. This provides the fractional cloud cover at three elevations: high (50–440 mb), middle (440–680 mb), and low (680–1000 mb), at 280-km resolution and monthly time scales. Only low and midlevel clouds are shown here, since these are the regions most affected by convective clouds and rainfall. ISCCP data were averaged over the period 1998–2001 for comparison to the model. Model output was aggregated to the same horizontal grid as the ISCCP data. To match up the vertical resolution, the model output was aggregated in the vertical assuming random overlap of clouds between layers, using layers 2–8 (roughly 760–1000 mb) for the low clouds and layers 9–12 (roughly 450–700 mb) for the middle clouds.

5. Results and discussion

a. Cloud fraction

Figures 4 and 5 show the time-mean low and midlevel cloud cover. The figures compare all six of the 4-yr (1998–2001) simulations presented in this study to the ISCCP data and illustrate the first-order effect of the new autoconversion parameterization. The figures show that GFC-Auto and EMAN-Auto simulations (see Table 4 for simulation names and characteristics) have significantly less low and middle cloud cover than GFC-New and EMAN-New. The difference is especially dramatic for EMAN-Auto. For both convection schemes, the previous overestimation bias in low cloud cover relative to ISCCP is significantly reduced in the Auto simulations, and the middle cloud is reduced to levels comparable to that of the Mod simulations.

These results suggest that 1) the new autoconversion method is significantly more efficient at producing rainfall and dissipating cloud cover than the default methods in RegCM3, and 2) the reasonable match between the default convective cloud cover (in GFC-Mod and EMAN-Mod) and ISCCP was the result of two compensating deficiencies: in creating the clouds (addressed in GFC-New and EMAN-New) and in dissipating the clouds via rainfall (addressed in GFC-Auto and EMAN-Auto). Hence the default cloud cover was reasonably close to ISCCP resulting from what could be considered a good combination of tuning. With the new formulations for convective cloud cover and autoconversion, the same cloud cover is produced but with much more physical realism. This has important ramifications for other aspects of the simulation, described further below.

Figures 6 and 7 present the mean diurnal cycle of the vertical structure of cloud cover averaged over land grid cells within the domain, for all six of the 4-yr (1998–2001) simulations presented in this study. The ocean cloud fraction is not shown since it does not exhibit a significant diurnal cycle. The figures show that the mid-level cloud cover that was prominent in GFC-New and EMAN-New is almost entirely removed in GFC-Auto and EMAN-Auto, again demonstrating the increased efficiency of the new autoconversion method in regions of high CLW. It is noted that the temperature falls below freezing at approximately 5-km elevation over this domain (not shown), and hence the midlevel cloud is mostly warm (i.e., liquid phase) and not in the presence of significant quantities of ice.

Figures 4 and 5 indicate that the time-mean cloud cover compared to ISCCP is not very different between the Mod and Auto simulations. But Figs. 6 and 7 clearly show that the diurnal cycles are shifted between these simulations such that the maximum low cloud cover occurs in the afternoon in GFC-Auto and EMAN-Auto rather than at night, as was the case for GFC-Mod and EMAN-Mod. This significantly impacts the simulation of radiative fluxes. Cloud fraction results from the 19-yr simulations are not shown here for brevity but were very similar to the 4-yr simulation results.

b. Radiative and turbulent heat fluxes

Figures 8 and 9 show the average diurnal cycle of incoming solar radiation (insolation) reaching the surface over land and ocean, comparing the SRB observations to all six of the 4-yr (1998–2001) simulations. Mean daily values are given in parentheses.

With GFC-Auto, insolation was slightly reduced relative to GFC-Mod and GFC-New, but not enough to remove the overestimation bias compared to SRB. Since the simulated low and midlevel fractional cloud cover in GFC-Auto compared well to ISCCP, it is likely that the overestimation of insolation is the result of insufficiently dense cloud cover, particularly at high elevations (not shown). This outcome is the result of weak convective updraft mass flux simulated by the Grell scheme, which is discussed in detail further below.

Over both land and ocean, EMAN-Auto simulates more insolation than EMAN-New but less than EMAN-Mod, resulting in a diurnal cycle of insolation that matches well to SRB. It is especially encouraging that the peak insolation is well simulated, both in magnitude and timing. These results illustrate the impact of reproducing a reasonable diurnal cycle of cloud cover on radiative fluxes.

The results from the 4-yr simulations using the Emanuel convection scheme indicate that combining the new parameterizations for convective cloud fraction and

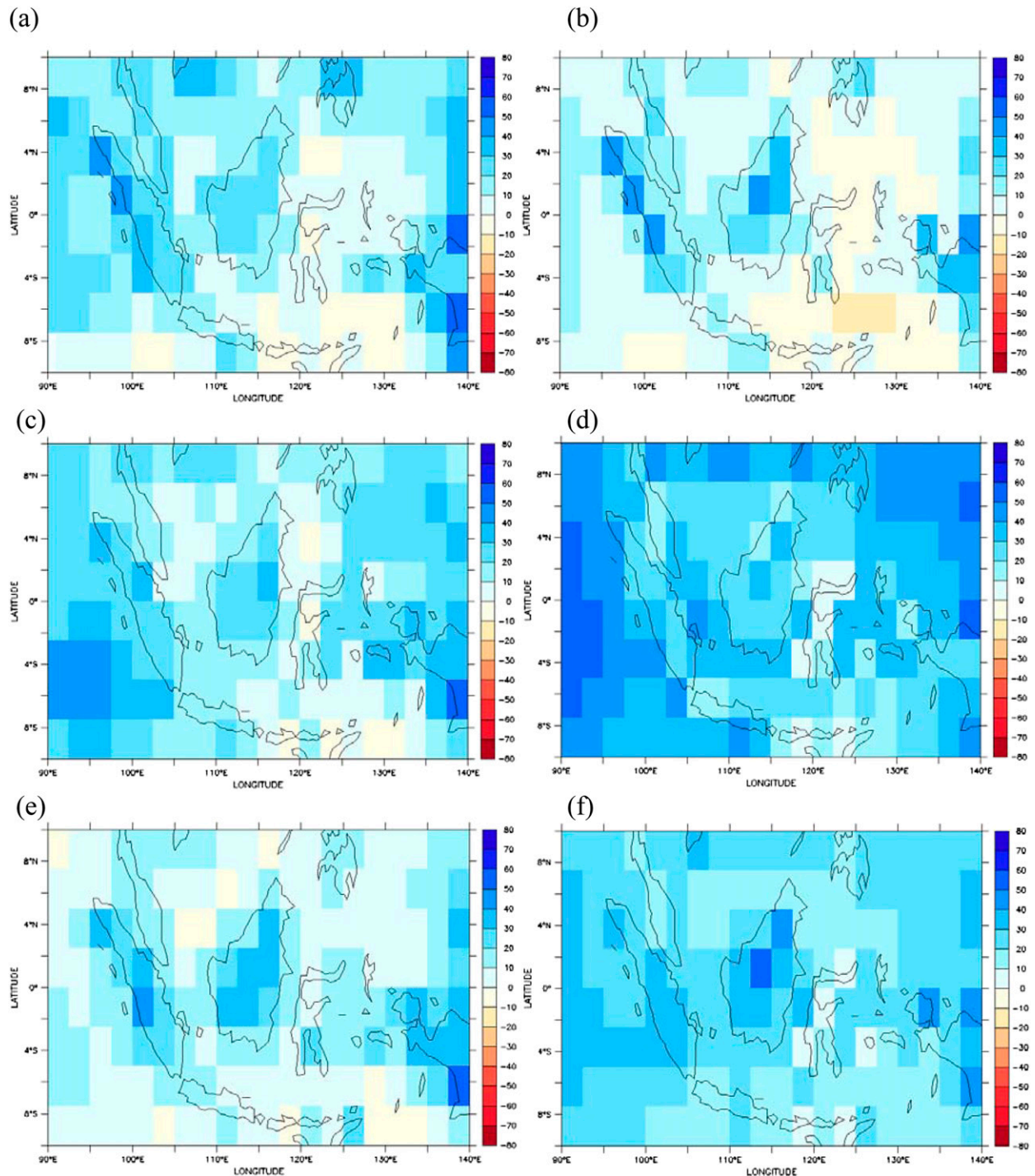


FIG. 4. Average low cloud fraction for 1998–2001: simulation minus ISCCP for (a) GFC-Mod, (b) EMAN-Mod, (c) GFC-New, (d) EMAN-New, (e) GFC-Auto, and (f) EMAN-Auto. Color bar indicates fractional coverage of grid cell.

autoconversion result in good simulation of both cloud cover and insolation. To validate that these model improvements hold over the 19-yr evaluation period and that other performance metrics are similarly improved, Table 5 summarizes the average daily surface radiative

and turbulent heat fluxes for the period 1983–2001 for the EMAN-Def_Long and EMAN-Auto_Long simulations compared to the observations.

Over land, EMAN-Def_Long significantly overestimates insolation at the earth's surface. This occurs

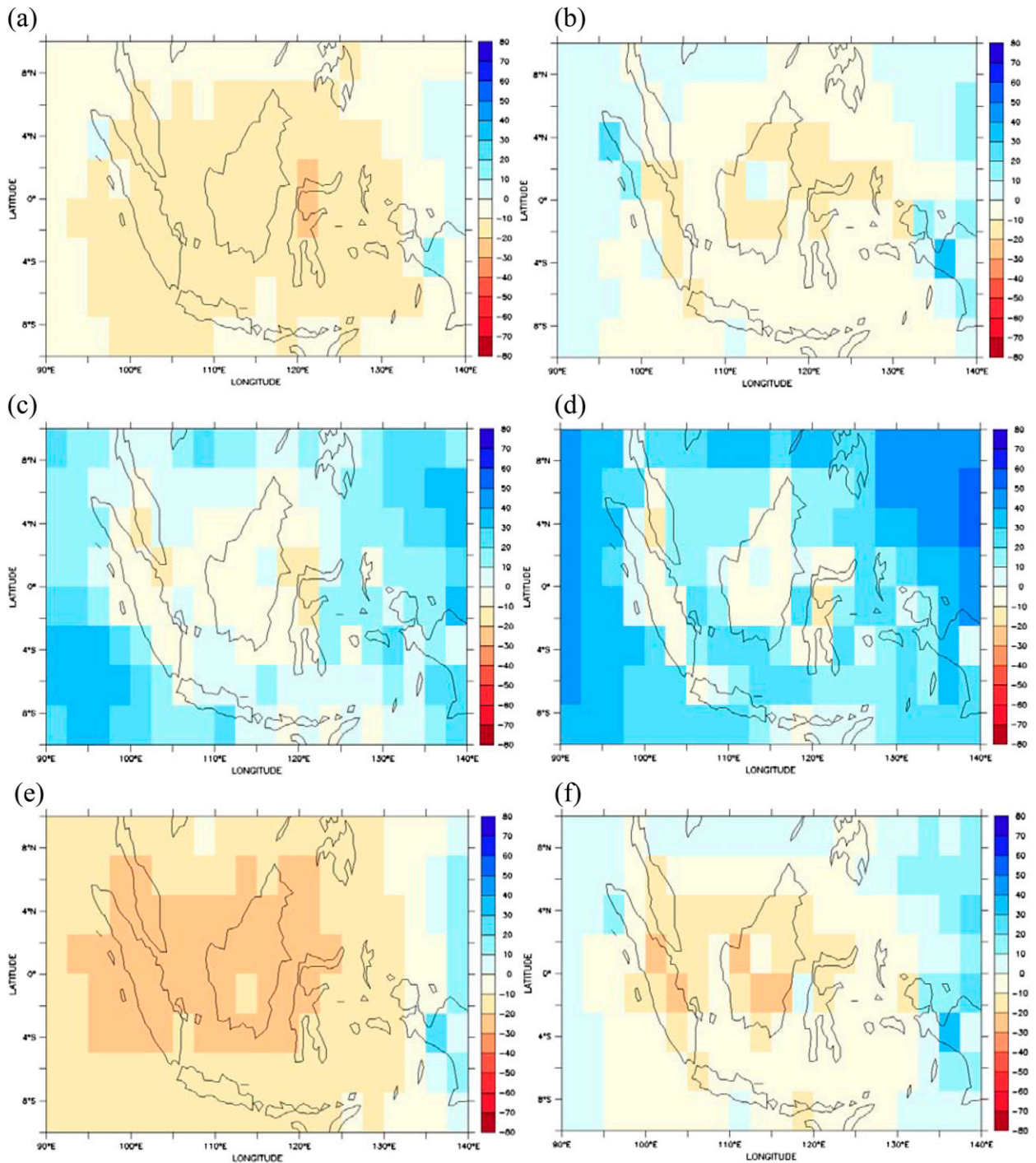


FIG. 5. As in Fig. 4, but for average middle cloud fraction.

despite good simulation of the planetary albedo and propagates into error in the simulated net radiation and the latent and sensible heat flux (LH and SH). But with EMAN-Auto_Long, simulated insolation matches very well to SRB. There is a small underestimation of planetary

albedo. EMAN-Auto_Long has a small underestimation of net radiation, primarily because of a combination of small errors in the simulated longwave radiation. Both EMAN-Def_Long and EMAN-Auto_Long show underestimation error in SH, although the bias is reduced

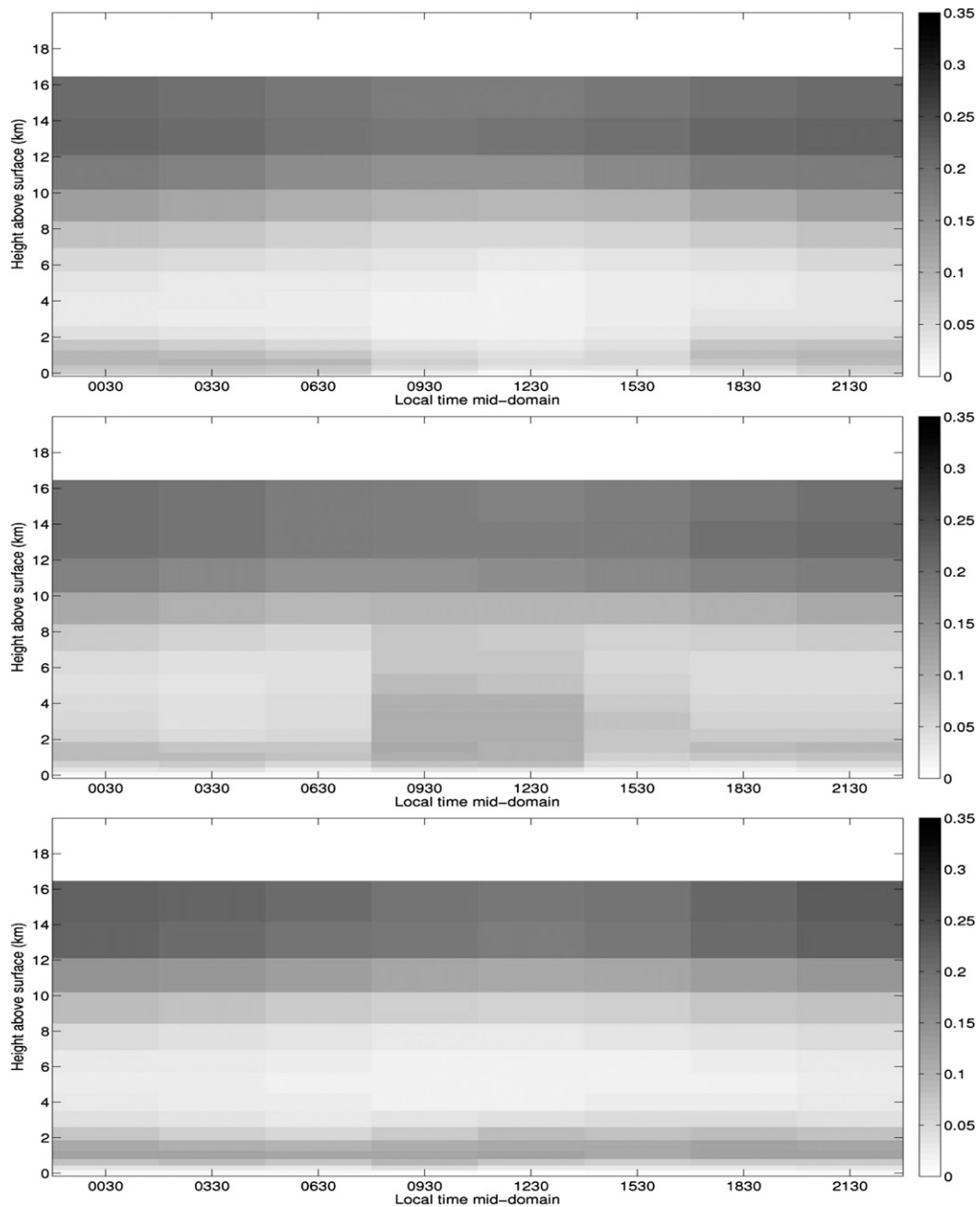


FIG. 6. Diurnal cycle of cloud cover averaged over land grid cells within the model domain for period 1998–2001 using simulations (top) GFC-Mod, (middle) GFC-New, and (bottom) GFC-Auto. The x -axis labels indicate the time of the middle of each 3-h output window, with respect to local time in the center of the model domain. To represent the y axis on a linear scale, the vertical extent of each model layer was assigned a single value of cloud cover, as provided by the model output. In reality, a smoother profile with less abrupt vertical variability would be expected.

in EMAN-Auto_Long. This error most likely stems from the IBIS land surface scheme, not the atmospheric component of RegCM3.

Over ocean, the results from EMAN-Auto_Long also show considerable improvement in the simulation of

insolation, with a very good match to observations and removal of the significant overestimation bias that was present in EMAN-Def_Long. There is a small underestimation of net radiation with EMAN-Auto_Long, again primarily because of small errors in the longwave

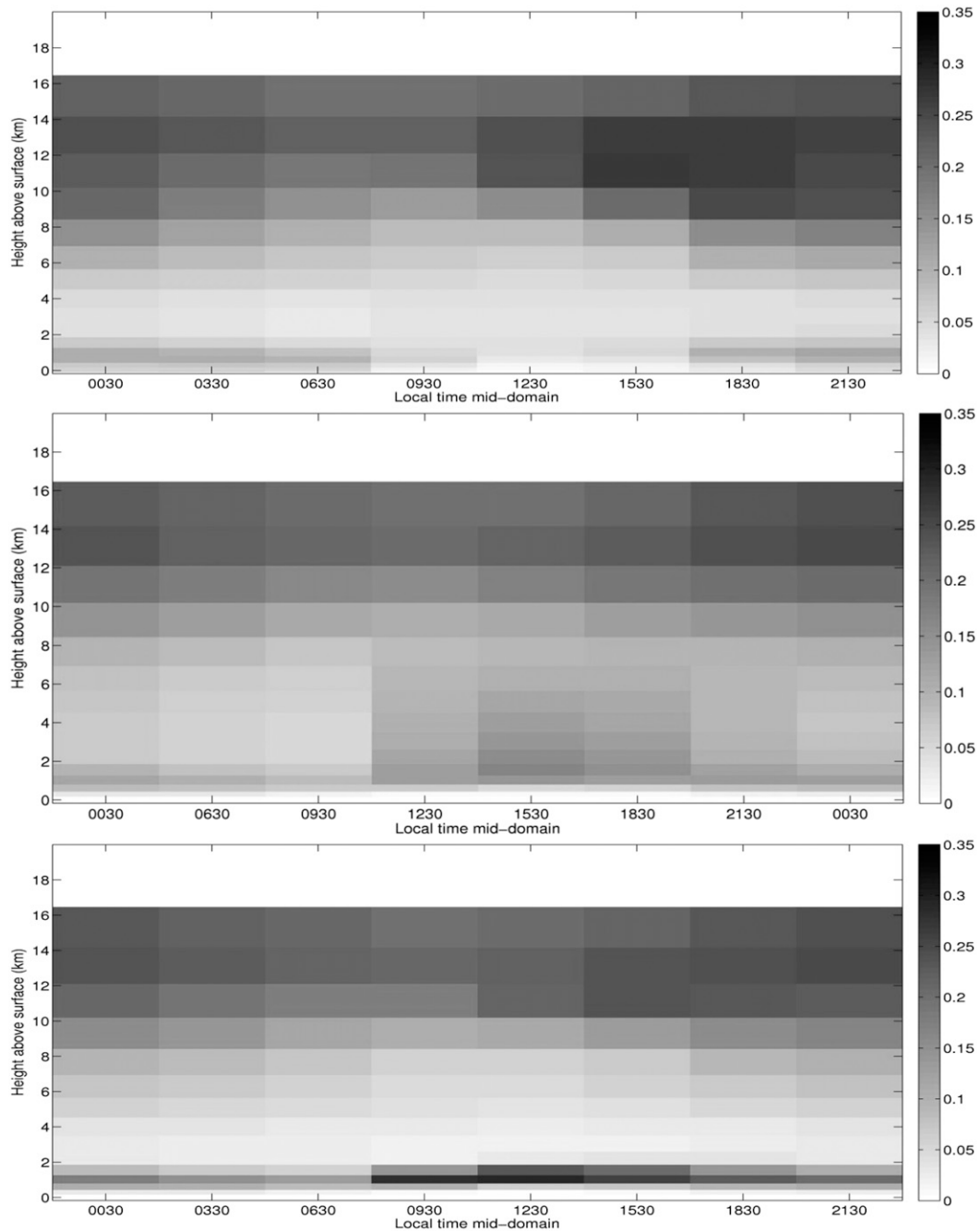


FIG. 7. As for Fig. 6, but using simulations (top) EMAN-Mod, (middle) EMAN-New, and (bottom) EMAN-Auto.

radiation. The simulated overestimation of LH and underestimation of SH in EMAN-Def_Long is not addressed in EMAN-Auto_Long. It is considered that this is because SSTs are fixed in these simulations, and hence turbulent heat fluxes over ocean exhibit little sensitivity to the surface net radiation. However, if an ocean model were coupled to the new RegCM3-IBIS model, it is expected that simulated turbulent fluxes over

the ocean would show improvement relative to the default version of RegCM3.

Therefore these results indicate that improvements to the simulated diurnal cycle of cloud cover and insolation propagate into improvements in the mean radiative and turbulent heat fluxes over longer time periods, when using the Emanuel convection scheme.

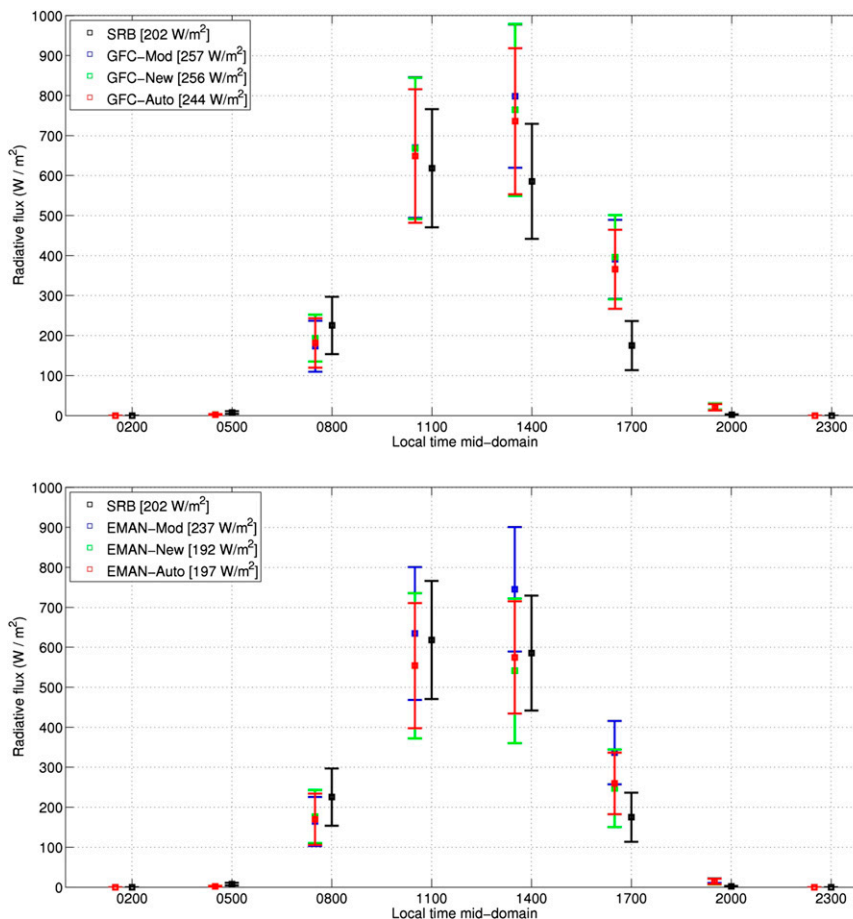


FIG. 8. Diurnal cycle of incoming solar radiation averaged over land for period 1998–2001 for SRB observations and simulations using (top) Grell with Fritsch-Chappell and (bottom) Emanuel convection schemes. Square symbol indicates the mean value; error bars indicate ± 1 standard deviation.

c. Rainfall

Table 6 shows the mean total, convective, and large-scale rainfall volumes for simulations evaluated over the period 1998–2001. The results show divergent behavior between the two convection schemes in response to the new autoconversion function.

GFC-Auto shows a reduction in convective rainfall compared to GFC-Mod and GFC-New, leading to an underestimation of convective and total rainfall over both land and ocean that was not present in the default version of RegCM3, resulting in worse model performance than the original version of this scheme (see Gianotti et al. 2012). This result seems inconsistent with the decrease in cloud cover and insolation that resulted from the new autoconversion method and is somewhat counterintuitive. The reasons for this are discussed in the next section.

EMAN-Auto shows an increase in convective rainfall relative to EMAN-New, but produces less rainfall than

in EMAN-Mod. This result is consistent with the shift in diurnal timing of cloud cover resulting from the new convective cloud fraction and associated change to insolation. The simulated convective and total rainfall volumes produced by EMAN-Auto are a reasonable match to TRMM over both land and ocean, showing considerable improvement on the previous simulations using the Emanuel scheme. These results indicate that the new autoconversion function, combined with the new convective cloud fraction, leads to improved physical realism throughout the simulation when using this scheme.

Table 6 also displays the total rainfall volumes and estimated convective and large-scale rainfall fractions produced by the 19-yr simulations. The results confirm that the new methods lead to improved model performance with respect to rainfall using the Emanuel scheme.

d. Implications of using different convection schemes

Differences in model performance between the Grell and Emanuel convection schemes result from very

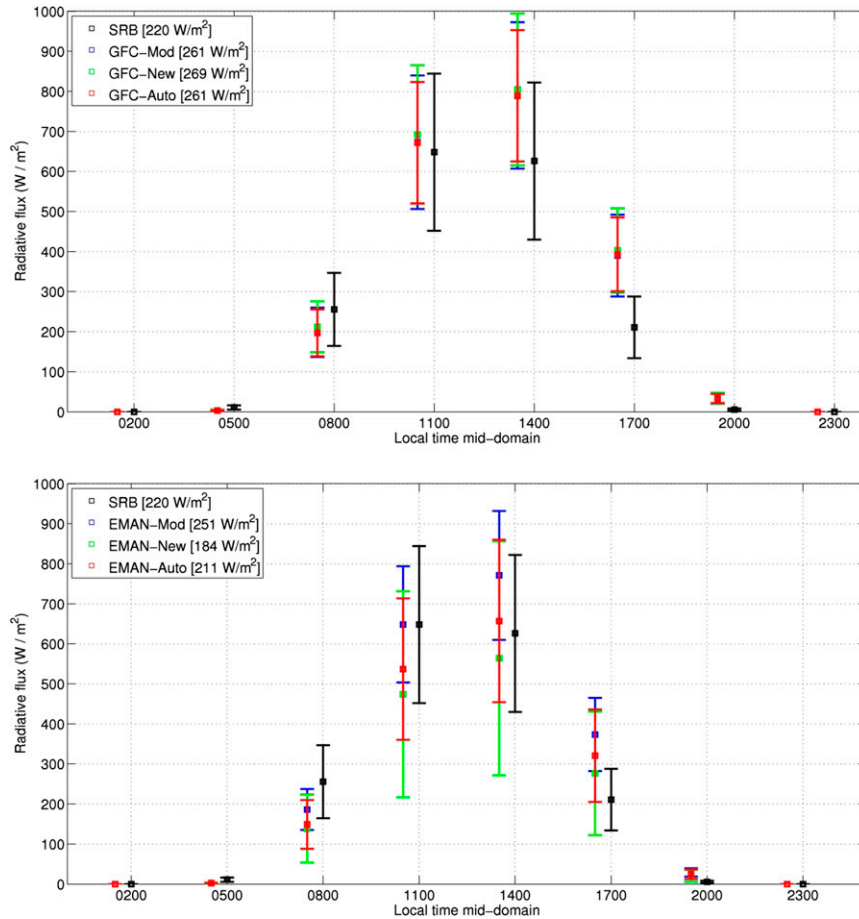


FIG. 9. As in Fig. 8, but for diurnal cycle of incoming solar radiation averaged over ocean.

different approaches to simulating convective updraft mass flux. The work presented here indicates that it is important to consider the implications of each scheme in the context of the Maritime Continent and other regions where convection is a dominant feature.

In both schemes, the volume of convective rainfall received at the surface is the product of the updraft mass flux and the amount of precipitable water produced in each model layer through the vertical column, minus any

reevaporation of rainfall that occurs between the cloud and the ground. Model testing showed that the amount of CLW produced from the available moisture within each grid cell was similar between the two schemes, as were the rates of reevaporation. Hence the primary cause of the difference in convective rainfall between the Grell and Emanuel schemes was the simulation of updraft mass flux.

In the Emanuel scheme, the updraft mass flux is a function of the degree of instability at the lifting

TABLE 5. Average daily surface radiation and turbulent heat fluxes over the period 1983–2001 for (top) land and (bottom) ocean cells within the domain. All radiative and turbulent fluxes are in units of $W m^{-2}$.

Product/simulation	SW _{dn}	SW _{up}	SW _{net}	Land albedo	Planetary albedo	LW _{dn}	LW _{up}	R _N	LH	SH
Land										
Observations	207	28	180	13%	47%	410	452	138	95	43
EMAN-Def_Long	226	32	195	14%	48%	412	460	147	126	22
EMAN-Auto_Long	208	30	179	14%	44%	406	457	128	100	29
Ocean										
Observations	225	14	211	6%	44%	419	466	164	102	8
EMAN-Def_Long	271	17	254	6%	43%	412	471	194	118	5
EMAN-Auto_Long	226	15	211	7%	46%	419	471	159	119	5

TABLE 6. Average daily rainfall over land and ocean for observations and simulations evaluated over (top) 1998–2001 and (bottom) 1983–2001. All values are in units of mm day^{-1} .

Product/simulation	Land average			Ocean average		
	Total	Convective	Large-scale	Total	Convective	Large-scale
1998–2001						
TRMM	8.6	5.4 (63%)	3.2 (37%)	7.0	4.0 (57%)	3.0 (43%)
GFC-Mod	10.9	4.4 (40%)	6.5 (60%)	8.5	4.1 (48%)	4.4 (52%)
GFC-New	9.2	4.1 (45%)	5.1 (55%)	7.3	5.5 (75%)	1.8 (25%)
GFC-Auto	5.9	3.1 (52%)	2.8 (48%)	4.8	2.9 (61%)	1.9 (39%)
EMAN-Mod	16.8	9.9 (59%)	6.9 (41%)	6.7	3.8 (57%)	2.9 (43%)
EMAN-New	10.3	5.0 (49%)	5.3 (51%)	7.9	3.5 (44%)	4.4 (56%)
EMAN-Auto	9.9	5.4 (55%)	4.5 (45%)	6.1	3.7 (61%)	2.4 (39%)
1983–2001						
Observations*	7.2	4.5 (63%)	2.7 (37%)	5.7	3.2 (57%)	2.5 (43%)
EMAN-Def_Long	10.3	6.6 (64%)	3.7 (36%)	3.9	3.2 (82%)	0.7 (18%)
EMAN-Auto_Long	7.3	4.5 (62%)	2.8 (38%)	4.0	2.6 (65%)	1.4 (35%)

* Total rainfall volumes are taken from GPCP data; convective and large-scale rainfall fractions are taken from TRMM data as described in Mori et al. (2004) and applied to the GPCP rainfall volume.

condensation level (LCL), as measured by the difference in density temperature between a lifted air parcel and the environment at that time step (Emanuel 1991). This makes convection with the Emanuel scheme very sensitive to changes in the near-surface environment, such that convective rainfall directly reflects lower atmospheric instability.

Updraft mass flux in the Grell scheme is based on the cloud work function, which is an integral measure of the buoyancy energy available for convection and provides the necessary closure for the scheme. The updraft mass flux is derived based on the assumption that the cloud work function is in quasi-equilibrium, such that the time rate of change of the total cloud work, which is a function of both the large-scale variables and the modification of the environment because of the cumulus cloud ensemble, is approximately zero (Arakawa and Schubert 1974). For both the large-scale and cumulus cloud components, the cloud work is a function of the moist static energy in the updraft compared to the downdraft. The result of this assumption is that updraft mass flux and convective rainfall increase (decrease) if the updraft strength increases (decreases) relative to the downdraft.

This study illustrates the impact of these different approaches to updraft mass flux. When rainfall efficiency is increased using the Emanuel scheme, cloud cover decreases and insolation increases, creating more instability in the lower atmosphere and consequently stronger updraft mass flux. This creates a positive feedback loop that leads to increased rainfall. However, when rainfall efficiency is increased using the Grell scheme, this dries out the atmosphere and strengthens the downdraft, leading to a decrease in the net convective mass flux and producing less total rainfall at the surface.

In developing their cumulus parameterization, Arakawa and Schubert (1974) used a time-integrated updraft mass flux that represented the mean cloud mass flux over the life time of a cumulus cloud ensemble, taken to be the time scale for moist convective adjustment. This time scale was shown to be on the order of 10^3 – 10^4 s (from 30 min to 3 h), significantly smaller than the time scale of the large-scale processes that create the instability driving convection, which is on the order of 10^5 s (about 1 day) (Arakawa and Schubert 1974).

The convective adjustment time scale was intended to be virtually instantaneous in the sense that it is basically the same as the computational time step for implementing the physics (Arakawa 2004). It is noted that the GCMs into which the original Arakawa and Schubert (1974) scheme was originally implemented were of resolution 100–200 km, with a computational time step on the order of hours, suitable for assuming an almost instantaneous adjustment due to convection.

However, an RCM running at the scale of tens of kilometers typically has a time step of a few minutes. Hence a single computational time step only represents a fraction of the cloud lifetime, substantially less than that required to assume “instantaneous” convective adjustment. Therefore the time-averaged mass flux used in the Arakawa and Schubert (1974) scheme is not considered appropriate for simulations that require a description of the time evolution of convection. The Emanuel scheme, on the other hand, achieves adjustment toward quasi-equilibrium during the time integration of explicitly formulated transient processes (Arakawa 2004). Therefore it is suggested that the Grell scheme is not suitable for RCM simulations but the Emanuel scheme is well suited to RCM simulations,

especially over regions of strong convection and given appropriate radiative forcing as shown in this work.

6. Summary

This paper describes a new parameterization for convective autoconversion that can be used within large-scale climate models, and evaluates the new method using the coupled regional model RegCM3-IBIS. The new method is derived from observed distributions of cloud water content and is constrained by observations of cloud droplet characteristics and climatological rainfall intensity. This method explicitly accounts for sub-grid variability with respect to cloud cover and cloud water density. It is spatially and temporally variable and independent of model resolution.

Simulations over the Maritime Continent using the Emanuel convection scheme showed improvement in model performance across a broad range of metrics, including cloud cover, radiative fluxes, and rainfall. The wet bias simulated by the default Emanuel scheme over land was greatly reduced without creating a dry bias over the ocean. The land to ocean rainfall ratio simulated by EMAN-Mod was 2.5:1, while the ratio simulated by EMAN-Auto was 1.6:1—a significant improvement compared to the observed ratio of 1.2:1 shown by TRMM.

The improvements in model performance with the Emanuel scheme held not only over a 4-yr evaluation period but also over a 19-yr validation period. If the model modifications were the result of parameter tuning over the initial 4-yr period, then longer simulations would not necessarily exhibit reasonable performance. Additionally, all the model modifications tested here were aimed at improving the representation of diurnal-scale processes, but model performance was improved over much longer time scales. These results support the assertion that poor representation of the diurnal cycle is a major source of error in climate simulations over the Maritime Continent.

Simulations with the Grell convection scheme produced counterintuitive results of increased rainfall efficiency but decreased total rainfall production. The results illustrate some of the limitations of the quasi-equilibrium theory for moist convective adjustment, as embodied in the Grell scheme, when used in a model with a relatively small time step over a region where convection is a dominant feature.

There are likely to be other important feedbacks of these new formulations for cloud cover and autoconversion that are not documented here, such as sensitivity to different large-scale forcings. When coupled to an ocean model, instead of being forced with SSTs as in this study, it is also likely that the new formulations

for cloud cover and autoconversion will produce very different results than the default version of the model. Ongoing work will evaluate the model performance over regions other than the Maritime Continent and coupled to an ocean model.

Acknowledgments. Funding for this study was provided by the Singapore National Research Foundation through the Singapore-MIT Alliance for Research and Technology (SMART) Center for Environmental Sensing and Modeling (CENSAM). RLG was also supported by the MIT Martin Family Society of Fellows for Sustainability. The authors are grateful to Filippo Giorgi and one anonymous reviewer for comments that helped to improve the manuscript.

REFERENCES

- Adler, R. F., and Coauthors, 2003: The version 2 Global Precipitation Climatology Project (GPCP) monthly precipitation analysis (1979–present). *J. Hydrometeorol.*, **4**, 1147–1167.
- Arakawa, A., 2004: The cumulus parameterization problem: Past, present, and future. *J. Climate*, **17**, 2493–2525.
- , and W. H. Schubert, 1974: Interaction of a cumulus cloud ensemble with the large-scale environment, Part I. *J. Atmos. Sci.*, **31**, 674–701.
- Bergman, J. W., and M. L. Salby, 1996: Diurnal variations of cloud cover and their relationship to climatological conditions. *J. Climate*, **9**, 2802–2820.
- Blossey, P. N., C. S. Bretherton, J. Cetrone, and M. Kharoutdinov, 2007: Cloud-resolving model simulations of KWAJEX: Model sensitivities and comparisons with satellite and radar observations. *J. Atmos. Sci.*, **64**, 1488–1508.
- Brenguier, J.-L., H. Pawlowska, L. Schüller, R. Preusker, J. Fischer, and Y. Fouquart, 2000: Radiative properties of boundary layer clouds: Droplet effective radius versus number concentration. *J. Atmos. Sci.*, **57**, 803–821.
- Chow, K. C., J. C. L. Chan, J. S. Pal, and F. Giorgi, 2006: Convection suppression criteria applied to the MIT cumulus parameterization scheme for simulating the Asian summer monsoon. *Geophys. Res. Lett.*, **33**, L24709, doi:10.1029/2006GL028026.
- Christensen, J. H., and Coauthors, 2007: Regional climate projections. *Climate Change 2007: The Physical Science Basis*. S. Solomon et al., Eds., Cambridge University Press, 847–940.
- Dai, A., and K. E. Trenberth, 2004: The diurnal cycle and its depiction in the Community Climate System Model. *J. Climate*, **17**, 930–951.
- Davies, H., and R. Turner, 1977: Updating prediction models by dynamical relaxation: An examination of the technique. *Quart. J. Roy. Meteor. Soc.*, **103**, 225–245.
- Del Genio, A. D., M.-S. Yao, W. Kovari, and K. K.-W. Lo, 1996: A prognostic cloud water parameterization for global climate models. *J. Climate*, **9**, 270–304.
- Eltahir, E. A. B., and R. L. Bras, 1993: Estimation of the fractional coverage of rainfall in climate models. *J. Climate*, **6**, 639–644.
- Emanuel, K. A., 1991: A scheme for representing cumulus convection in large-scale models. *J. Atmos. Sci.*, **48**, 2313–2335.
- , 1994: *Atmospheric Convection*. Oxford University Press, 580 pp.

- , and M. Živković-Rothman, 1999: Development and evaluation of a convection scheme for use in climate models. *J. Atmos. Sci.*, **56**, 1766–1782.
- Foster, J., M. Bevis, and W. Raymond, 2006: Precipitable water and the lognormal distribution. *J. Geophys. Res.*, **111**, D15102, doi:10.1029/2005JD006731.
- Fowler, L. D., D. A. Randall, and S. A. Rutledge, 1996: Liquid and ice cloud microphysics in the CSU general circulation model. Part I: Model description and simulated microphysical processes. *J. Climate*, **9**, 489–529.
- Francisco, R. V., J. Argete, F. Giorgi, J. Pal, X. Bi, and W. J. Gutowski, 2006: Regional model simulation of summer rainfall over the Philippines: Effect of choice of driving fields and ocean flux schemes. *Theor. Appl. Climatol.*, **86**, 215–227.
- Fritsch, J. M., and C. F. Chappell, 1980: Numerical prediction of convectively driven mesoscale pressure systems. Part I: Convective parameterization. *J. Atmos. Sci.*, **37**, 1722–1733.
- Geoffroy, O., J.-L. Brenguier, and I. Sandu, 2008: Relationship between drizzle rate, liquid water path and droplet concentration at the scale of a stratocumulus cloud system. *Atmos. Chem. Phys. Discuss.*, **8**, 3921–3959.
- Gianotti, R. L., 2012: Convective cloud and rainfall processes over the Maritime Continent: Simulation and analysis of the diurnal cycle. Ph.D. dissertation, Massachusetts Institute of Technology, 306 pp.
- , and E. A. B. Eltahir, 2014: Regional climate modelling over the Maritime Continent. Part I: New parameterization for convective cloud fraction. *J. Climate*, **27**, 1488–1503.
- , D. Zhang, and E. A. B. Eltahir, 2012: Assessment of the Regional Climate Model version 3 over the Maritime Continent using different cumulus parameterization and land surface schemes. *J. Climate*, **25**, 638–656.
- Giorgi, F., and Coauthors, 2012: RegCM4: Model description and preliminary tests over multiple CORDEX domains. *Climate Res.*, **52**, 7–29.
- Global Soil Data Task, IGDP-DIS, 2000: Global soil data products CD-ROM. International Geosphere-Biosphere Programme, Data and Information System (IGDP-DIS), Potsdam, Germany. [Available online at <http://daac.ornl.gov/SOILS/igbp.html>.]
- Grell, G. A., 1993: Prognostic evaluation of assumptions used by cumulus parameterizations. *Mon. Wea. Rev.*, **121**, 764–787.
- , J. Dudhia, and D. R. Stauffer, 1994: Description of the fifth-generation Penn State/NCAR Mesoscale Model (MM5). NCAR Tech. Rep. TN-398+STR, 117 pp.
- Holtlag, A. A. M., and B. A. Boville, 1993: Local versus nonlocal boundary-layer diffusion in a global climate model. *J. Climate*, **6**, 1825–1842.
- , E. I. F. de Bruijn, and H.-L. Pan, 1990: A high-resolution air mass transformation model for short-range weather forecasting. *Mon. Wea. Rev.*, **118**, 1561–1575.
- Huffman, G. J., and Coauthors, 2007: The TRMM Multisatellite Precipitation Analysis (TMPA): Quasi-global, multiyear, combined-sensor precipitation estimates at fine scales. *J. Hydrometeorol.*, **8**, 38–55.
- Iassamen, A., H. Sauvageot, N. Jeannin, and S. Ameer, 2009: Distribution of tropospheric water vapor in clear and cloudy conditions from microwave radiometric profiling. *J. Appl. Meteor. Climatol.*, **48**, 600–615.
- Kessler, E., 1969: *On the Distribution and Continuity of Water Substance in Atmospheric Circulations*. *Meteor. Monogr.*, No. 32, Amer. Meteor. Soc., 84 pp.
- Khain, A., M. Ovtchinnikov, M. Pinsky, A. Pokrovsky, and H. Krugliak, 2000: Notes on the state-of-the-art numerical modeling of cloud microphysics. *Atmos. Res.*, **55**, 159–224.
- Khairoutdinov, M. F., and D. A. Randall, 2003: Cloud resolving modeling of the ARM summer 1997 IOP: Model formulation, results, uncertainties, and sensitivities. *J. Atmos. Sci.*, **60**, 607–625.
- Kubar, T. L., D. L. Hartmann, and R. Wood, 2009: Understanding the importance of microphysics and macrophysics for warm rain in marine low clouds. Part I: Satellite observations. *J. Atmos. Sci.*, **66**, 2953–2972.
- Lord, S. J., 1982: Interaction of a cumulus cloud ensemble with the large-scale environment. Part III: Semi-prognostic test of the Arakawa–Schubert cumulus parameterization. *J. Atmos. Sci.*, **39**, 88–103.
- Manton, M. J., and W. R. Cotton, 1977: Formulation of approximate equations for modeling moist deep convection on the mesoscale. Atmospheric Science Paper 266, Colorado State University, Fort Collins, 62 pp.
- Marshall, J. S., and W. McK. Palmer, 1948: The distribution of raindrops with size. *J. Meteor.*, **5**, 165–166.
- Martin, G. M., M. A. Ringer, V. D. Pope, A. Jones, C. Dearden, and T. J. Hinton, 2006: The physical properties of the atmosphere in the new Hadley Centre Global Environmental Model (HadGEM1). Part I: Model description and global climatology. *J. Climate*, **19**, 1274–1301.
- Mori, S., and Coauthors, 2004: Diurnal land–sea rainfall peak migration over Sumatera Island, Indonesian Maritime Continent, observed by TRMM satellite and intensive rawinsonde soundings. *Mon. Wea. Rev.*, **132**, 2021–2039.
- Neale, R. B., and J. Slingo, 2003: The Maritime Continent and its role in the global climate: A GCM study. *J. Climate*, **16**, 834–848.
- , and Coauthors, 2010: Description of the NCAR Community Atmosphere Model (CAM 4.0). NCAR Tech. Note NCAR/TN-485+STR, 212 pp.
- Pal, J. S., E. E. Small, and E. A. B. Eltahir, 2000: Simulation of regional-scale water and energy budgets: Representation of subgrid cloud and precipitation processes within RegCM. *J. Geophys. Res.*, **105** (D24), 579–594.
- , and Coauthors, 2007: Regional climate modeling for the developing world: The ICTP RegCM3 and RegCNET. *Bull. Amer. Meteor. Soc.*, **88**, 1395–1409.
- Ramankutty, N., 1999: Estimating historical changes in land cover: North American croplands from 1850 to 1992. *Global Ecol. Biogeogr.*, **8**, 381–396.
- Rangno, A. L., and P. V. Hobbs, 2005: Microstructures and precipitation development in cumulus and small cumulonimbus clouds over the warm pool of the tropical Pacific Ocean. *Quart. J. Roy. Meteor. Soc.*, **131**, 639–673.
- Reid, J. S., P. V. Hobbs, A. L. Rangno, and D. A. Hegg, 1999: Relationships between cloud droplet effective radius, liquid water content, and droplet concentration for warm clouds in Brazil embedded in biomass smoke. *J. Geophys. Res.*, **104** (D6), 6145–6153.
- Reynolds, R. W., N. Rayner, T. Smith, D. Stokes, and W. Wang, 2002: An improved in situ and satellite SST analysis for climate. *J. Climate*, **15**, 1609–1625.
- Rogers, R. R., and M. K. Yau, 1989: *A Short Course in Cloud Physics*. Elsevier, 293 pp.
- Rosenfeld, D., and I. M. Lensky, 1998: Satellite-based insights into precipitation formation processes in continental and maritime convective clouds. *Bull. Amer. Meteor. Soc.*, **79**, 2457–2476.
- , and C. W. Ulbrich, 2003: Cloud microphysical properties, processes, and rainfall estimation opportunities. *Radar and*

- Atmospheric Science: A Collection of Essays in Honor of David Atlas, Meteor. Monogr.*, No. 52, Amer. Meteor. Soc., 237–258.
- Rossow, W. B., A. W. Walker, D. E. Beusichel, and M. D. Roiter, 1996: International Satellite Cloud Climatology Project (ISCCP) documentation of new cloud datasets. WMO/TD-No. 737, 115 pp.
- Rotstajn, L. D., 2000: On the “tuning” of autoconversion parameterizations in climate models. *J. Geophys. Res.*, **105** (D12), 15 495–15 507.
- Squires, P., 1958: The microstructure and colloidal stability of warm clouds. Part II: The causes of the variations in microstructure. *Tellus*, **10**, 262–271.
- Stackhouse, P. W., Jr., S. K. Gupta, S. J. Cox, J. C. Mikořitz, T. Zhang, and L. M. Hinkelman, 2011: 24.5-year SRB data set released. *GEWEX News*, No. 21, International GEWEX Project Office, Silver Spring, MD, 10–12.
- Stephens, G. L., and J. M. Haynes, 2007: Near global observations of the warm rain coalescence process. *Geophys. Res. Lett.*, **34**, L20805, doi:10.1029/2007GL030259.
- Sundqvist, H., E. Berge, and J. E. Kristjánsson, 1989: Condensation and cloud parameterization studies with a mesoscale numerical weather prediction model. *Mon. Wea. Rev.*, **117**, 1641–1657.
- Testud, J., S. Oury, R. A. Black, P. Amayenc, and X. Dou, 2001: The concept of “normalized” distributions to describe raindrop spectra: A tool for cloud physics and cloud remote sensing. *J. Appl. Meteorol.*, **40**, 1118–1140.
- Tiedtke, M., 1993: Representation of clouds in large-scale models. *Mon. Wea. Rev.*, **121**, 3040–3061.
- Ulbrich, C., 1983: Natural variations in the analytical form of the raindrop size distribution. *J. Climate Appl. Meteor.*, **22**, 1764–1775.
- United States Geological Survey, 1996: Global 30-arc second elevation dataset (GTOPO30). [Available online at http://eros.usgs.gov/#/Find_Data/Products_and_Data_Available/gtopo30_info.]
- Uppala, S. M., and Coauthors, 2005: The ERA-40 Re-Analysis. *Quart. J. Roy. Meteor. Soc.*, **131**, 2961–3012. [Dataset available online at <http://www.ecmwf.int/research/era/do/get/era-40>.]
- Wang, Y., L. Zhou, and K. Hamilton, 2007: Effect of convective entrainment/detrainment on the simulation of the tropical precipitation diurnal cycle. *Mon. Wea. Rev.*, **135**, 567–585.
- Warner, J., 1955: The water content of cumuliform cloud. *Tellus*, **7**, 449–457.
- Winter, J. M., J. S. Pal, and E. A. B. Eltahir, 2009: Coupling of Integrated Biosphere Simulator to Regional Climate Model version 3. *J. Climate*, **22**, 2743–2757.
- Xu, K.-M., and Coauthors, 2005: Modeling springtime shallow frontal clouds with cloud-resolving and single-column models. *J. Geophys. Res.*, **110**, D15S04, doi:10.1029/2004JD005153.
- Yang, G.-Y., and J. Slingo, 2001: The diurnal cycle in the tropics. *Mon. Wea. Rev.*, **129**, 784–801.
- Yu, L., X. Jin, and R. A. Weller, 2008: Multidecade global flux datasets from the objectively analyzed air-sea fluxes (OAFlux) project: Latent and sensible heat fluxes, ocean evaporation, and related surface meteorological variables. Woods Hole Oceanographic Institution OAFlux Project Tech. Rep. OA-2008-01, 64 pp. [Available online at http://oafux.whoi.edu/pdfs/OAFlux_TechReport_3rd_release.pdf.]